



Polyvinyl alcohol/Montmorillonite/Zirconium Phosphate Nanocomposite Film as potent matrix in Scaffold-guided Tissue Engineering Application

¹Manoj Patowary, ²Himani Kalita

¹Assistant Professor, ²Researcher

¹School of Computing,

¹MIT-ADT University, Pune, Maharashtra, India

²Department of Chemistry,

²SP Pune University, Pune, Maharashtra, India

Abstract: Development of suitable matrix is vital in scaffold-guided tissue engineering application that could aid in cellular growth for tissue regeneration. Herein, nanocomposite film of polyvinyl alcohol (PVA)/montmorillonite (MMT)/zirconium phosphate (ZP) has been synthesized as potential matrix for scaffold-guided tissue engineering application via solvent casting method, where PVA was used as the polymer matrix, while MMT as well as ZP nanoparticles were used as the reinforcing bioactive fillers. The prepared nanocomposite film was characterized by various spectroscopic as well as microscopic techniques. The nanocomposite exhibits significant mechanical properties as observed in the nanoindentation tests (hardness = 0.1234 GPa and elastic modulus = 3.94 GPa at a load of 500 μ N), while *in-vitro* cellular studies on the nanocomposite film using mouse 3T3 fibroblast cells revealed its superior bioactivity, thereby substantiating its applicability as a potential matrix in scaffold-guided tissue engineering application. Additionally, the nanocomposite displayed a controlled biodegradation rate in phosphate buffered saline (PBS) medium containing lysozymes with a residual mass > 62% on the 30th day. The developed nanocomposite also exhibits a controlled swelling behavior.

IndexTerms - Nanocomposite; scaffold; tissue engineering; bioactivity; mechanical property.

1. INTRODUCTION

Designing and development of suitable scaffolds is one of the most important steps involved in the sequence process of tissue engineering, which combines the principles of molecular biology and engineering [1] with the aim of restoring and regenerating the damaged tissues/organs. Accordingly, the scaffolds must exhibit good bioactivity, biodegradability, and biocompatibility and must provide sufficient mechanical support to maintain stresses and loadings generated during *in-vitro/in-vivo* tissue regeneration. In most of the nanocomposite scaffold guided tissue engineering application, the desired enhancement in mechanical properties is often achieved by the incorporation of suitable filler materials into polymeric matrix of the nanocomposites. The fillers, usually organic/inorganic materials such as clays, metal nanoparticles, etc., are reported to tailor the mechanical properties of nanocomposite scaffolds over a wide range by acting as molecular bridges in the polymer matrix of the nanocomposite, resulting in improved mechanical properties [2]. In this regard, nanoparticles of zirconium phosphate (ZP) are expected to serve as promising bioactive filler in the fabrication of nanocomposite scaffolds, owing to their excellent biocompatibility, wide availability and thermal as well as chemical inertness. Besides, the presence of phosphates in ZP is believed to support cellular proliferation owing to their biomimetic behavior [3-4]. Nonetheless, to the best of our knowledge, ZP has not been much reported and studied as bioactive filler in the fabrication of nanocomposite scaffolds to date. Apart from nanoparticles, bioinert clay filler such as montmorillonite [MMT; $(\text{Na,Ca})_{0.33}(\text{Al,Mg})_2(\text{Si}_4\text{O}_{10})(\text{OH})_2 \cdot n\text{H}_2\text{O}$] is also reported to improve the bioactivity [5-6] as well as mechanical properties [7] of polymer nanocomposites owing to its high surface area and large aspect ratio. In view of the properties of the mentioned fillers, the present work, therefore, attempts to combine bioactive filler ZP, bioinert clay filler MMT, and biocompatible as well as biodegradable polymer polyvinyl alcohol (PVA) to fabricate nanocomposite film for potential usage as matrix material in scaffold-guided tissue engineering application with improved mechanical properties and superior bioactivity. Both ZP and MMT are expected to act as reinforcing bioactive fillers for improving the mechanical properties and bioactivity of PVA. In literature, it has been reported that ZP (layered α -ZP) significantly enhances the mechanical properties of PVA in PVA/ZP nanocomposites in contrast to neat PVA [8]. Further, various literature reports available on the synthesis of PVA/MMT composites showed that the usage of MMT as filler significantly improves the mechanical properties of the composites [9-12]. However, the bioactivity and applicability of the hybrid nanocomposites in tissue engineering was not investigated so far.

Albeit, PVA has been studied in numerous biomedical applications such as in drug delivery [13-15], tendon repair [16], tissue engineering [17-19], contact lens [20], etc., its limitation of aqueous instability needs to be surmounted by using crosslinkers. However, the use of crosslinkers such as glutaraldehyde [21], maleic acid [22], boric acid [23], maleic anhydride

[24], etc. could result in toxic side effects, thereby limiting the suitability of the crosslinked polymer for biomedical applications. Hence, the selection of non-toxic crosslinker is very important for fabricating water insoluble PVA nanocomposite scaffold for clinical usage. In the current work, non-toxic malic acid was used as the chemical crosslinker to fabricate the nanocomposite film via solvent casting method. For comparison, nanocomposite films of PVA/ZP and PVA/MMT were also developed. The prepared nanocomposites were characterized by various spectroscopic and microscopic techniques. Nanomechanical properties of the nanocomposites have been appraised through nanoindentation tests, while their bioactivity was assessed via various *in-vitro* cell culture experiments using mouse 3T3 fibroblast cells. The biodegradability as well as swelling behavior of the nanocomposites has also been investigated.

2. EXPERIMENTAL

2.1. CHEMICALS

Zirconium oxychloride octahydrate was purchased from S.D. Fine-Chem Limited (India), while orthophosphoric acid, copper sulfate pentahydrate and DL-malic acid were procured from Merck (India). Cetyltrimethylammonium bromide (CTAB) was bought from Spectrochem Private Limited (India). Montmorillonite (MMT) K10 was obtained from Alfa Aesar, whereas polyvinyl alcohol (PVA; mol. wt. 125,000) was purchased from Central drug house (P) Limited (India). 3-(4, 5-dimethylthiazol-2-yl)-2, 5-diphenyltetrazolium bromide (MTT) and bichinchonic acid (BCA) were obtained from Sigma-Aldrich, while Dulbecco's modified Eagle's medium (DMEM), fetal bovine serum (FBS), antibiotic agent, and Hoechst 33342 were obtained from Gibco. 3T3 fibroblast cells were obtained from the National Center for Cell Science (NCCS), Pune (India). All the chemicals were used as received without any further purification.

2.2. PREPARATION OF ZIRCONIUM PHOSPHATE NANOPARTICLES

Zirconium phosphate nanoparticles were prepared as reported elsewhere [25]. For the synthesis, zirconium oxychloride (1 mmol) was added to an aqueous solution of CTAB (0.1 mmol) followed by the addition of orthophosphoric acid (2 mmol) under continuous stirring. After that, the mixture was sonicated using a probe sonicator for 2 h with pulse on and off mode for 5 and 1 s respectively. Finally, the white colored product was collected, washed three times with water, dried at 70 °C for 12 h, and calcined at 700 °C for 4 h to get the fine powder of zirconium phosphate (ZP) nanoparticles.

2.3. PREPARATION OF PVA NANOCOMPOSITE FILMS

The PVA nanocomposite films were prepared by solvent casting method. For preparing the nanocomposite film of PVA and ZP, an aqueous PVA solution (7% w/v) was prepared by heating the solution at 80 °C. 1 wt% of ZP nanoparticles were dispersed in 2 mL water and then added to the aqueous PVA solution. The solution was stirred at the same temperature for 4 h to get a homogenous mixture. Finally, the mixture was poured into petri dish (90 mm diameter) placed on a leveled surface and transferred to a vacuum oven at 70 °C for 12 h to get dried thin film (thickness of ~0.4 mm). The dried nanocomposite film was named as PVA-ZP.

For preparing the nanocomposite film of PVA and MMT, 2 wt% of MMT (dispersed in 2 mL water) was added to aqueous PVA solution (7% w/v), followed by the above mentioned procedure. The film, thus obtained, was designated as PVA-MMT.

Similarly, for preparing the nanocomposite film of PVA, MMT, and ZP an aqueous PVA solution (7% w/v) was prepared to which 2 wt% MMT (dispersed in 2 mL water) was added followed by the addition of 1 wt% ZP nanoparticles (dispersed in 2 mL water). The dried thin film, obtained by following the procedure as mentioned above, was nomenclated as PVA-MMT-ZP. For comparison, neat PVA film was also prepared. All the nanocomposite films as well as the neat PVA film were chemically crosslinked with 10 wt% malic acid to increase their stability in aqueous medium, where the crosslinker was added to the initial homogeneous mixtures.

2.4. CHARACTERIZATION OF THE NANOPARTICLES AND NANOCOMPOSITE FILMS

X-ray diffraction (XRD) pattern of the samples were obtained from Bruker AXS Diffractometer D8 Powder XRD by using Cu-K α radiation at a scan rate of 3° min⁻¹ with a sampling interval of 0.05 at 40 mA and 40 kV. Functional group analyses of the prepared nanoparticles and nanocomposite films were performed by fourier transform infra-red (FT-IR) spectroscopy using Thermo Scientific Nicolet 6700 FT-IR instrument (model NEXUS- 870). Thermal analyses of the nanocomposites were performed using Netzsch STA 409 PC Luxx (Germany). Transmission electron microscopic (TEM) analysis was performed using JEM-2100 HRTEM (JEOL, Japan) operating at 200 kV, whereas scanning electron microscopic (SEM) analyses were performed using ZEISS EVO 60 Scanning Electron Microscope (Germany). Atomic force microscopic (AFM) analyses were performed using Agilent Technologies USA: AFM 5500.

2.5. NANOINDENTATION TESTS

Nanoindentation experiments were performed to determine the nanomechanical properties of the nanocomposites using Nano-Triboindenter (TI 950 TriboIndenter, Hysitron Inc., USA) equipped with a three-sided pyramidal diamond indenter tip (Berkovich type) of radius 150 nm. The nanoindentation tests were performed in load control mode at three different loads of 500, 800 and 1000 μ N with a dwell time of 10 s for all the tests. The loading and unloading time during the tests was 10 s each. All the samples were subjected to a minimum of 10 indents and the results obtained were an average of these indentations.

The hardness (H) and reduced modulus (E_r) of the nanocomposites was calculated from the load versus displacement data using the Oliver and Pharr method [26], which is the standard method of analysis for nanoindentation testing. According to Oliver and Pharr method, hardness and modulus were calculated using the following relations:

$$H = P_{\max}/A \quad (1)$$

where, H is the hardness, P_{\max} is maximum indentation force and A is the contact area, which is a function of contact depth (h_c) given by

$$h_c = h_{\max} - 0.75 (P_{\max}/S) \quad (2)$$

where, h_{\max} is the maximum depth, P_{\max} is maximum indentation force, S is the contact stiffness, and 0.75 is a constant value for Berkovich indenter.

$$E_r = \frac{\sqrt{\pi}}{2\sqrt{A}} \times S \quad (3)$$

where, E_r is the reduced modulus, A is the contact area and S is the contact stiffness.

2.6. SWELLING STUDIES

The medium uptake or swelling studies of the samples (i.e. PVA nanocomposite films) were performed at 37 °C in phosphate buffered saline (PBS, pH 7.4) to determine the diffusion of medium and nutrients into the nanocomposites. For the study, the samples were weighed (dry weight) and immersed in PBS for a time period of 72 h. At predetermined time intervals of 1, 2, 6, 24, 48, and 72 h, the samples were carefully removed from the medium and dried using filter paper. Subsequently, the samples were weighed to determine their wet weight. The swelling ratio of the nanocomposites in the respective time periods was calculated using equation 4.

$$\text{Swelling ratio} = \frac{\text{wet weight} - \text{dry weight}}{\text{dry weight}} \quad (4)$$

Swelling ratio of neat PVA film was similarly studied in PBS at time periods of 1, 2, 6, 24, 48, and 72 h. Each experiment was repeated three times and the average value was taken to validate the results.

2.7. IN-VITRO DEGRADATION STUDIES

The *in-vitro* degradation of the nanocomposites in physiological condition was studied in PBS containing 10 µg/mL lysozymes (hen egg-white, Sigma-Aldrich) at a pH of 7.4. For the studies, the samples were weighed and immersed in the solution of PBS and lysozyme for a period of 30 days at 37 °C. To retain the enzymatic activity, the solution mixture was replaced after every third day. At predetermined time intervals of 10, 15, 20, 25, and 30 days, the samples were removed from the solution, washed with distilled water, and dried under vacuum. Subsequently, the dried samples were weighed and the amount of *in-vitro* degradation of the nanocomposites was expressed as % residue of the samples, which was calculated using equation 5.

$$\text{Residual mass (\%)} = (W_f/W_i) \times 100\% \quad (5)$$

where, W_f is the weight of the dried sample after immersion in PBS containing lysozyme solution and W_i is the initial weight of the sample. All the experiments were performed in triplicate.

2.8. CELL CULTURE STUDY ON THE NANOCOMPOSITES

The cell culture studies were performed with mouse fibroblast (3T3) cells cultured in complete DMEM containing 10% FBS and 1% antibiotic agent (penicillin-streptomycin), maintained at a temperature of 37 °C and 5% CO₂ in a humidified incubator.

For cell culture studies, the nanocomposites were initially sterilized by immersion in 70% ethanol for 1 h, after which they were taken out from the medium, washed repeatedly with PBS and incubated in DMEM media for 12 h. Finally, the samples were placed in tissue culture plate (TCP) and 3T3 fibroblast cells were seeded onto them at a cell density of 1×10^4 cells/well. Cells seeded into the well of TCP without any sample were used as the positive control. After seeding the cells, the TCP was incubated at 37 °C and the culture medium was replaced every 24 h. All the samples were taken in triplicate for performing the cell culture experiments.

2.9. IN-VITRO CELL VIABILITY, PROLIFERATION, ADHESION AND MORPHOLOGY ASSAY

2.9.1. MTT ASSAY

The viability and proliferation of 3T3 fibroblast cells on the nanocomposites were evaluated through MTT [3-(4,5-dimethylthiazol-2-yl)-2,5-diphenyltetrazolium bromide] assay at specified time intervals of 3, 5 and 7 days after seeding the cells on the samples. The quantification of cell viability by MTT assay is based on the ability of mitochondrial dehydrogenases of living cells to oxidize the tetrazolium salt [3-(4,5-dimethylthiazol-2-yl)-2,5-diphenyltetrazolium bromide] to a water insoluble purple formazan product. Hence, the amount of the purple formazan product is directly proportional to the number of metabolically active cells [27]. Briefly, the culture media was removed from the wells of TCP and the samples (attached with cells) were rinsed with PBS. After that, the samples were incubated in MTT solution (0.5 mg/mL in PBS) for 4 h at 37 °C and 5% CO₂. Finally, the formed formazan crystals were dissolved in DMSO (dimethyl sulfoxide) by shaking for 30 min and the absorbance of the solution was recorded at 570 nm using a Platescreen microplate reader (Recorders & Medicare Systems, India).

2.9.2. SEM ANALYSIS

The spreading, adhesion and morphological characteristics of the proliferating 3T3 fibroblast cells on the nanocomposites' surface were evaluated by SEM analysis at specified time period of 3, 5, and 7 days. For the analysis, the

samples (attached with cells) were rinsed with PBS, fixed with 2.5% glutaraldehyde in PBS for 30 min at 4 °C and finally dehydrated with ascending series of aqueous ethanol solutions (50-100%) at room temperature. The samples were vacuum dried to ensure complete drying. The fully dried samples were then gold coated (Polaron sputter coater, UK) and observed under SEM at an accelerating voltage of 10-20 kV.

2.9.3. FLUORESCENCE MICROSCOPY

The adhesion, proliferation and spreading of the fibroblast cells on the nanocomposites were further assessed through fluorescence microscopy at specified time period of 3, 5, and 7 days. For the fluorescent imaging study, the samples (attached with the cells) were taken out after the specified time periods and rinsed with PBS. Subsequently, the cells on the samples were fixed with 4% paraformaldehyde and then stained with Hoechst 33342 with manufacturer's instructions. Finally, the fluorescent images were acquired with Axio Observer Z1 (Carl Zeiss, Germany).

2.10. PROTEIN ADSORPTION STUDY

Protein adsorption studies were carried out for all the nanocomposites at scheduled time period of 3, 6, and 12 h using the bicinchoninic acid (BCA) protein assay method. For the studies, the samples were initially sterilized by immersion in 70% ethanol for 1 h. Subsequently, they were placed in tissue culture plate and incubated in 1 mL of 1:1 FBS/PBS solution at 37 °C. After pre-determined time period (viz. 3, 6, and 12 h), the samples were rinsed with PBS and BCA reagent was added to them. The BCA reagent was prepared using 50 parts of BCA and 1 part of 4% copper (II) sulphate solution. The absorbance of the BCA reagent was measured at 562 nm (using UV-1601, Shimadzu, Japan) to quantify the adsorption of protein by the nanocomposites. All the samples were taken in triplicate for the studies.

3. RESULTS AND DISCUSSION

3.1. CHARACTERIZATION OF THE ZP NANOPARTICLES

The crystalline phase and purity of the prepared ZP nanoparticles was verified by XRD analysis and the pattern (scanned over 2θ range of 10-80°) is depicted in Fig. 1a. The XRD pattern is found to be consistent with JCPDS file no. 85-0896 analogous to cubic zirconium pyrophosphate (ZrP_2O_7). The peaks observed at 2θ values of 18.6, 21.5, 24.1, 26.4, 30.6, 36.1, and 49.3° can be indexed to the (111), (200), (210), (211), (220), (311), and (024) crystal planes of zirconium pyrophosphate respectively. No additional peaks are observed in the XRD pattern revealing the purity of the sample.

The functional groups present in the ZP nanoparticles were analyzed by FT-IR spectroscopy. The FT-IR spectrum, depicted in Fig. 1b, shows a broad peak at 1102 cm^{-1} corresponding to asymmetric stretching mode of the P-O bond, while the peaks at 757 and 523 cm^{-1} represents the bending modes of the O-P-O bonds (ν_4 and ν'_4 respectively). The peaks at 3435 and 1625 cm^{-1} represent the stretching and bending vibrations of water molecules respectively.

Morphological analysis of the ZP nanoparticles was performed through TEM studies and the bright field TEM micrograph is shown in Fig. 1c. The TEM image shows aggregates of spherical particles with the smallest visible aggregate measuring ~48 nm. Agglomeration of the particles might have occurred due to the condensation reactions among the hydroxyl groups [28] present on the adjacent ZP nanoparticles during the synthesis or calcination process. The selected area electron diffraction (SAED) pattern of the ZP nanoparticles reveals their crystalline nature (inset of Fig. 1c), while the energy dispersive X-ray (EDS) spectrum (EDS attached with TEM) of the nanoparticles shows peaks for the expected elements of Zr, P, and O (Fig. 1d). The peak for carbon and copper arises from the carbon coated copper grids used for the analysis. The absence of any other peaks shows the purity of the prepared product.

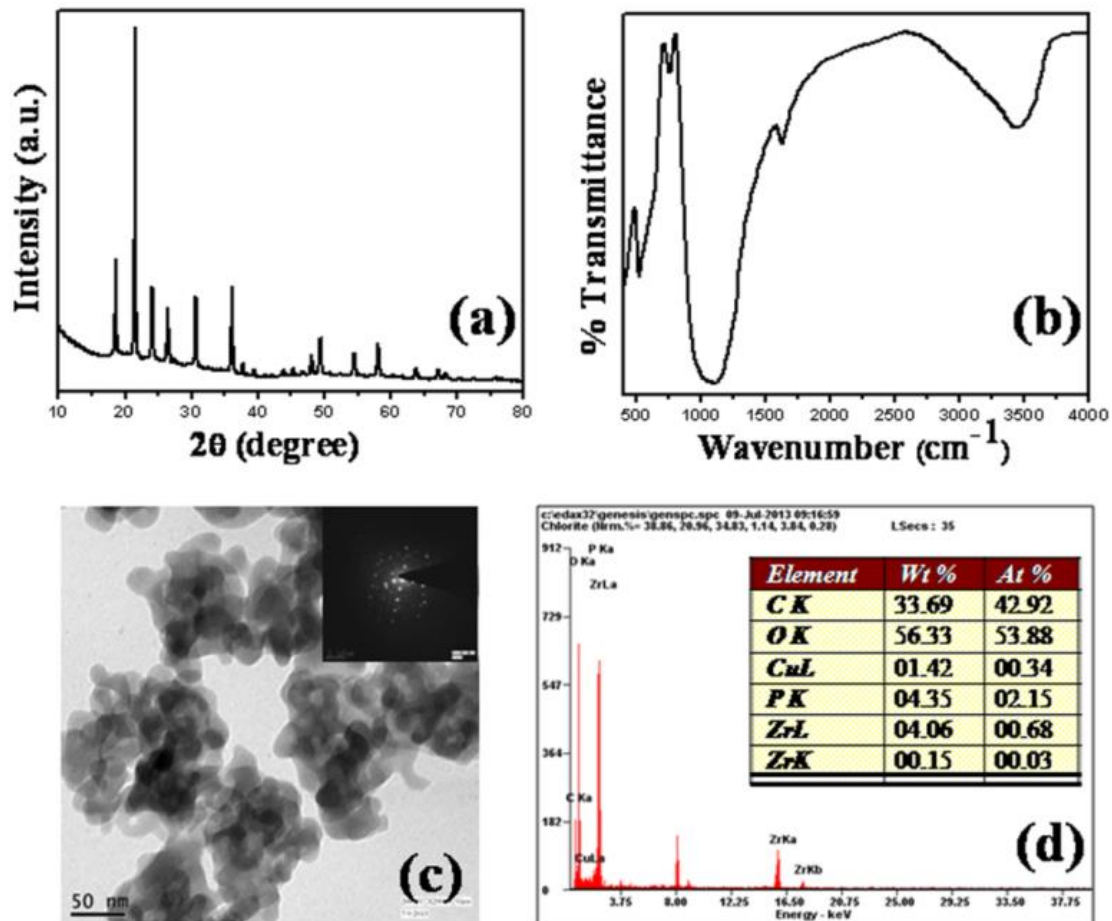


Fig. 1. (a) XRD, (b) FT-IR, (c) TEM, and (d) EDS spectrum of ZP nanoparticles (inset of (c): SAED pattern of the nanoparticles).

3.2. CHARACTERIZATION OF THE NANOCOMPOSITE FILMS

The XRD patterns of the PVA nanocomposites as well as the neat PVA film were scanned over 2θ range of $10\text{--}60^\circ$ and are depicted in Fig. 2. The XRD pattern of neat PVA film depicts an intense peak at 2θ value of 19.1° which corresponds to the crystalline phase [8] of PVA arising from the strong intermolecular hydrogen bonding between the PVA chains, whereas the small hump at 2θ value of 40.1° corresponds to an approximate hexagonal ordering of the PVA molecular chains [8]. Another smaller hump is observed at 2θ value of 22.2° . In the XRD pattern of the PVA nanocomposite films (viz. PVA-ZP, PVA-MMT, and PVA-MMT-ZP), the diffraction peak at 2θ values of 19.1 and 40.1° in neat PVA film are slightly shifted towards higher 2θ values. These shifts in the diffraction peaks suggest the interaction between the fillers (i.e. ZP and MMT) and PVA molecules in the nanocomposites. The diffraction peaks at 2θ value of 26.5 and 26.3° in the XRD pattern of PVA-MMT and PVA-MMT-ZP respectively corresponds to the crystalline phase of MMT.

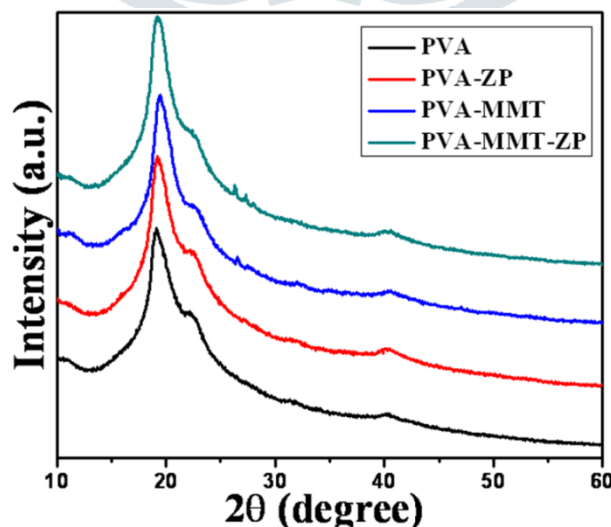


Fig. 2. XRD patterns of neat PVA and PVA nanocomposite films.

Functional group analyses of the crosslinked neat PVA as well as the PVA nanocomposite films were performed through attenuated total reflection-fourier transform infrared (ATR-FTIR) spectroscopy and the spectra are presented in Fig. 3.

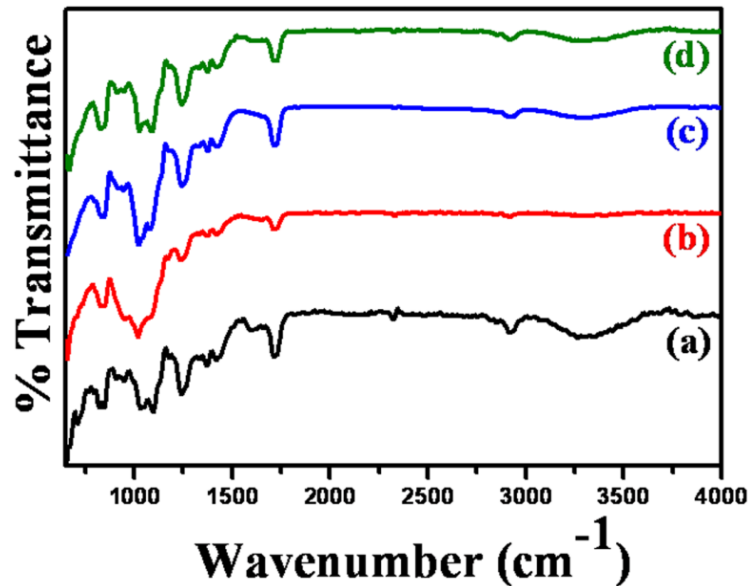


Fig. 3. FT-IR spectra of (a) neat PVA, (b) PVA-ZP, (c) PVA-MMT, and (d) PVA-MMT-ZP.

The FT-IR spectra of neat PVA film shows a broad band in the region of 3003-3600 cm^{-1} , which corresponds to the stretching vibration of the hydroxyl groups, whereas the band at 2916 cm^{-1} can be attributed to the stretching vibration of the alkyl C-H bond present in the PVA molecules. The strong band at 1712 cm^{-1} corresponds to the ester C=O stretching vibration, indicating the successful crosslinking of the PVA chains with malic acid via ester linkage between the hydroxyl and carboxyl groups of PVA and malic acid molecules respectively, as shown in the schematic diagram in Fig. 4. The FT-IR spectra for the PVA nanocomposite films are observed to be similar as the FT-IR spectrum for the neat PVA film. However, the spectra of the nanocomposite films are slightly shifted compared to neat PVA film, where the spectra for PVA-MMT and PVA-MMT-ZP are shifted to higher wavenumber values, while the spectrum for PVA-ZP is shifted to lower values. These shifts in the FT-IR spectra of the nanocomposite films might be due to the interaction between the fillers (i.e. ZP and MMT) and PVA molecules in the nanocomposites.

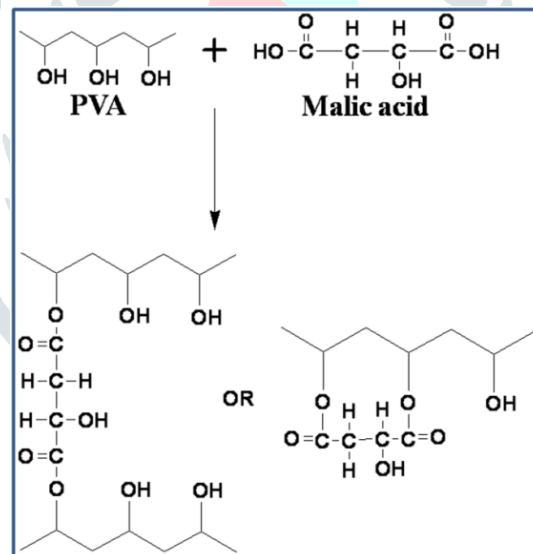


Fig. 4. Schematic diagram showing the crosslinking of PVA chains with malic acid via ester linkages.

The surface topography and roughness of the nanocomposites as well as the neat PVA film were analyzed by AFM and the images are shown in Fig. 5. The AFM images show few distinguishing features on the surface of the films with surface roughness (root mean square height, S_q) value of 0.974, 1.14, 1.63, and 1.69 nm for PVA, PVA-ZP, PVA-MMT, and PVA-MMT-ZP respectively. AFM analyses confirm the presence of surface nanoroughness in the films, which is an essential criterion of a scaffold for usage in tissue engineering application in providing the platform that facilitates the attachment of cells for proliferation.

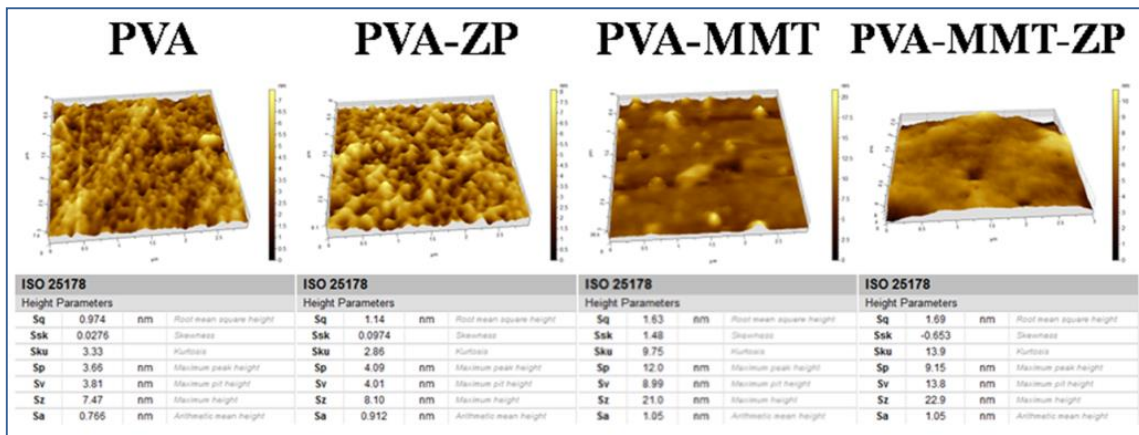


Fig. 5. AFM images of neat PVA and PVA nanocomposite films.

The distribution of fillers (i.e. ZP and MMT) in the polymer matrix of the nanocomposites was determined through SEM analyses and the images are depicted in Fig. 6. The SEM image of neat PVA film shows a clear surface, whereas SEM image of the nanocomposite films (viz. PVA-ZP, PVA-MMT, and PVA-MMT-ZP) shows a homogeneous distribution of the fillers (visible as white spots) in the polymer matrix. The uniform distribution indicates that the fillers interact well with PVA and hence are evenly dispersed in the polymer matrix in all the nanocomposites.

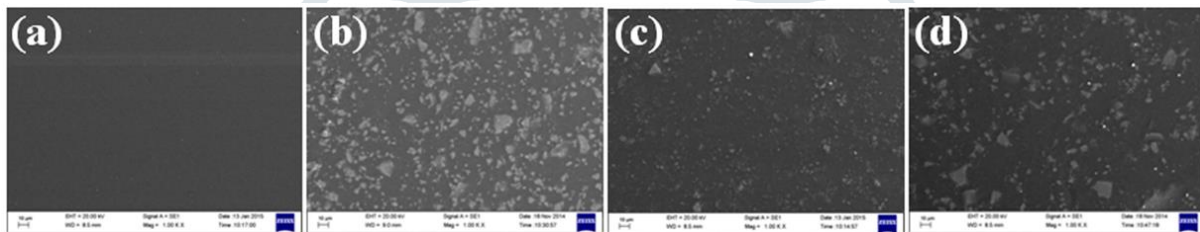


Fig. 6. SEM images of (a) neat PVA, (b) PVA-ZP, (c) PVA-MMT, and (d) PVA-MMT-ZP.

3.3. THERMAL PROPERTIES

The thermal stability of the nanocomposites was determined through thermogravimetric analysis (TGA) by heating the samples in alumina crucibles from 45 to 600 °C at a heating rate of 10 °C/min under nitrogen atmosphere. The TGA curves, shown in Fig. 7, show a three-step degradation process for all the PVA nanocomposites as well as for the neat PVA film. The first weight loss from 45 °C to ~175 °C corresponds to the loss of moisture from the films, whereas the second weight loss from ~195 °C to ~385 °C attributes to the decomposition of PVA structure. The final weight loss in the TGA curves corresponds to further degradation of the residuals [29-30]. Furthermore, it was observed that the degradation stages of the nanocomposites are shifted towards higher temperature as compared to the neat PVA film.

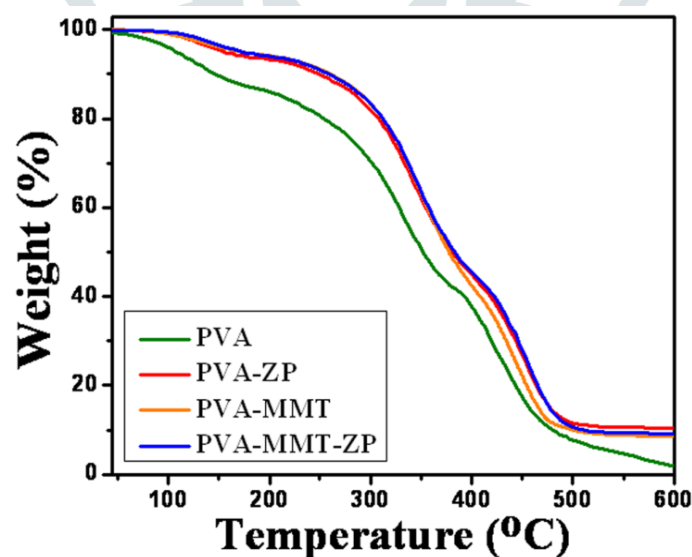


Fig. 7. TGA graphs of neat PVA and PVA nanocomposite films.

From the TGA graphs, two parameters are ascertained: the onset temperature at which 10% weight loss took place and the percentage residue left at 500 °C [31] and the data is summarized in Table 1. It was observed that the onset temperature for neat PVA film is 147 °C, whereas for the nanocomposites are 250, 260 and 259 °C for PVA-ZP, PVA-MMT, and PVA-MMT-ZP respectively. The shift in the degradation temperature to higher values indicates that the addition of filler molecules (ZP and MMT) improves the thermal stability of the nanocomposite films and creates a considerable delay in the weight loss, which is

probably due to the homogeneous dispersion of the fillers in the PVA matrix and presence of strong interaction between the fillers and PVA molecules, which suppress the polymer chain mobility.

Table 1 TGA results of neat PVA and PVA nanocomposite films.

Parameter	PVA	PVA-ZP	PVA-MMT	PVA-MMT-ZP
Temperature at 10% weight loss (°C)	147	250	260	259
Residue at 500 °C (wt%)	7.8	11.6	9.9	10.7

3.4. MECHANICAL PROPERTIES

The nanomechanical properties of the dry nanocomposite films were determined via load controlled nanoindentation tests at three different loads of 500, 800, and 1000 μN . The hardness and elastic modulus (reduced Young's modulus) values of the nanocomposites are shown in Fig. 8 and 9 respectively. For all the three loads, it was observed that both the hardness and elastic modulus values are highly enhanced on using ZP and MMT as fillers in contrast to the neat PVA film. Although the nanomechanical properties of PVA-ZP and PVA-MMT are much higher than that of the neat PVA film, but PVA-MMT-ZP (comprising both ZP and MMT as fillers) possesses the highest hardness and elastic modulus values among the three nanocomposites. This enhancement in the nanomechanical properties of the PVA nanocomposite films is due to the strong interfacial interaction between the PVA and filler (i.e. ZP and MMT) molecules resulting from the homogenous distribution of the fillers in the PVA matrix. The nanomechanical properties of the PVA nanocomposite films substantiate their applicability for usage as scaffolds in a variety of soft tissue engineering applications.

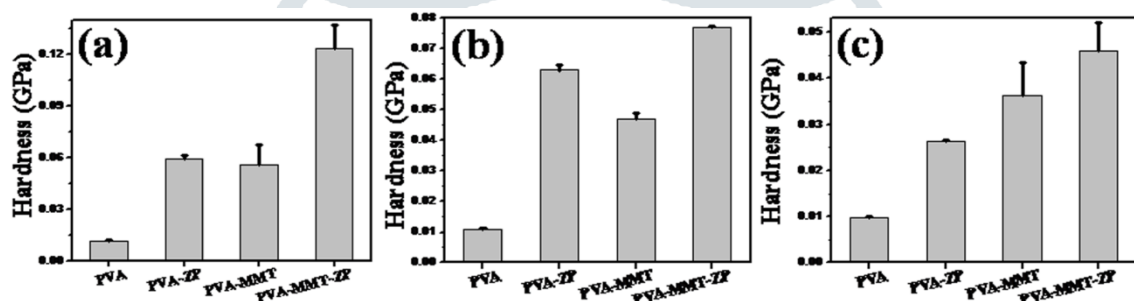


Fig. 8. Hardness values for the nanocomposites at the load of (a) 500, (b) 800, and (c) 1000 μN . Error bars represent the standard deviation from the mean (n=10).

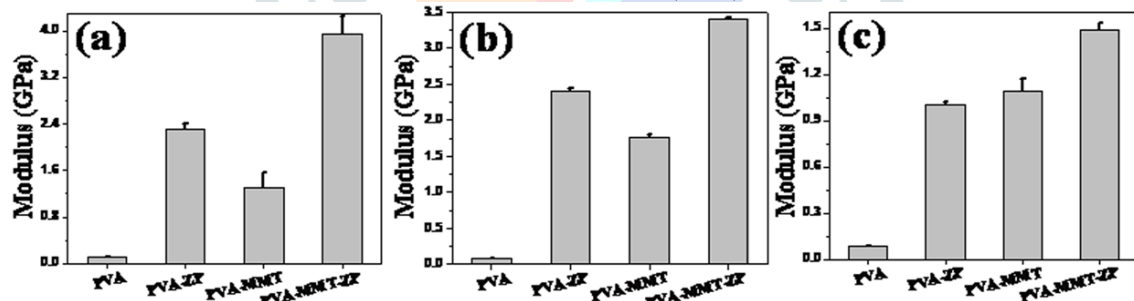


Fig. 9. Elastic modulus (reduced Young's Modulus) values for the nanocomposites at the load of (a) 500, (b) 800, and (c) 1000 μN . Error bars represent the standard deviation from the mean (n=10).

3.5. SWELLING STUDIES

Controlled swelling is an important parameter of a scaffold in tissue engineering application. The swelling of scaffolds facilitate the infiltration of cells into them, which helps in their proliferation and growth. Swelling also results in a larger surface area favoring the cellular adhesion and their growth in a three dimensional fashion. The swelling behavior of the PVA nanocomposite films are presented in Fig. 10a. It was observed that all the PVA nanocomposites as well as the neat PVA film exhibits rapid swelling in the initial 1 h of immersion in PBS solution, owing to the diffusion of solvent molecules into them. However, no considerable swelling was observed in the nanocomposites after 1 h, with the attainment of equilibrium over a period of 72 h. The filler molecules didn't produce any significant difference in the swelling ratio of the nanocomposites. Visual inspection also shows a substantial enhancement in the volume of the nanocomposites without any disintegration in the PBS medium, thereby maintaining their physical integrity. Thus, it can be inferred that the PVA nanocomposite films possess ideal swelling behavior vital for a scaffold in tissue engineering application.

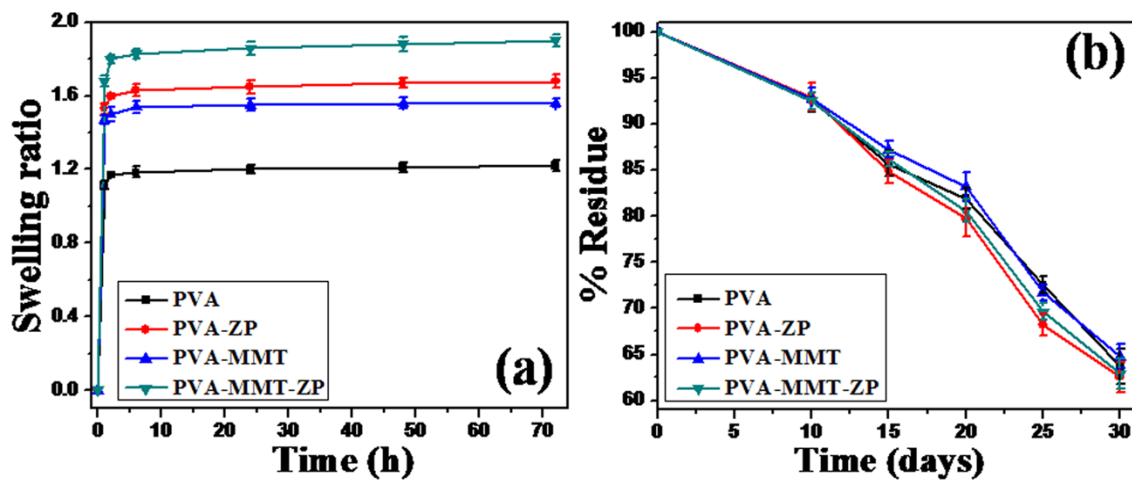


Fig. 10. (a) Swelling ratio and (b) *in-vitro* degradation studies of the nanocomposites. Error bars represent the standard deviation from the mean (n=3).

3.6. IN-VITRO DEGRADATION STUDIES

Biodegradability is an important parameter of a scaffold in tissue engineering application, which must be in a controlled manner so that its principle function of maintaining its mechanical strength during the formation of new tissues is fulfilled and new tissues are formed along with the degradation process, with the degraded remains either absorbed or eliminated from the body. The results of the *in-vitro* degradation studies of the nanocomposites, performed in PBS containing lysozymes, are presented in Fig. 10b. A gradual rate of degradation was observed in all the nanocomposites with residual mass >62% on the 30th day. Further, no substantial variation in the degradation rate of the nanocomposites was visible, which is possibly due to the similar degree of crosslinking of the PVA chains by malic acid through ester linkages. Moreover, the presence of fillers (viz. ZP and MMT) doesn't produce any detectable effect on the nanocomposites' degradation rate. The *in-vitro* degradation of the nanocomposites in the slightly alkaline medium of PBS containing lysozymes might have been aided by the basic and enzymatic hydrolysis of the ester linkages (formed during the crosslinking of PVA with malic acid) and the polymer (i.e PVA) backbone respectively. The *in-vitro* degradation study of the PVA nanocomposite films shows their controlled biodegradation behavior, which is crucial for a scaffold in tissue engineering application in supporting the formation of new tissues.

3.7. IN-VITRO CELL VIABILITY, PROLIFERATION, ADHESION AND MORPHOLOGY ASSAY

For tissue engineering application, a scaffold must be biocompatible and should support the adhesion as well as proliferation of cells on it. The results of MTT assay for evaluating the biocompatibility and cellular proliferation on the nanocomposites are presented in Fig. 11. It was observed that all the PVA nanocomposites as well as the neat PVA film don't exhibit any cytotoxic effect on the mouse fibroblast (3T3) cells and the cells maintained a good proliferation during the 7 day study period. A considerable increase in the number of viable cells was observed in all the nanocomposites in contrast to the control on the 7th day, which indicates their biocompatibility as well as their ability to support the proliferation of cells on them. The PVA nanocomposite films (viz. PVA-ZP, PVA-MMT, and PVA-MMT-ZP) show higher number of viable cells as compared to the neat PVA film, where the value is highest for PVA-MMT-ZP followed by PVA-MMT and PVA-ZP at the end of 7th day.

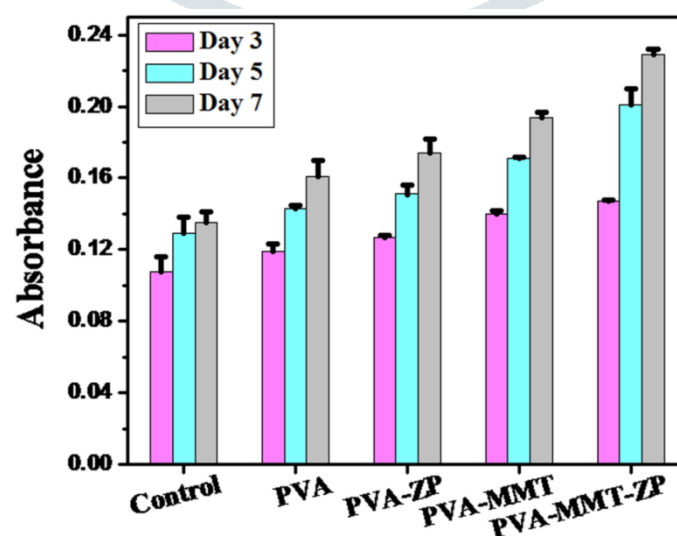


Fig. 11. MTT assay of the positive control and the nanocomposites. Error bars represent the standard deviation from the mean (n=3).

The attachment, morphology, spreading and proliferation of mouse fibroblast (3T3) cells on the nanocomposites was analyzed from the SEM images of the samples attached with the cells (Fig. 12) after 3, 5, and 7 days of culturing the cells. It was observed that there is a substantial increase in the attachment, spreading, and proliferation of the fibroblast cells on all the

nanocomposites with progressing time of cell culture. The irregular and flat-shaped cells on the nanocomposites' surface (on day three) proliferates and spreads to a larger area forming colonies of cells on day five and on succeeding days of cell culture. The attachment and spreading of the fibroblast cells was found to be highest on PVA-MMT-ZP film followed by PVA-MMT, PVA-ZP, and neat PVA film at the end of 7th day, thereby substantiating the results of MTT assay. Thus, it can be inferred that all the nanocomposites facilitates the attachment, spreading and proliferation of cells on their surface, which is probably aided by the nanoroughness of their surfaces.

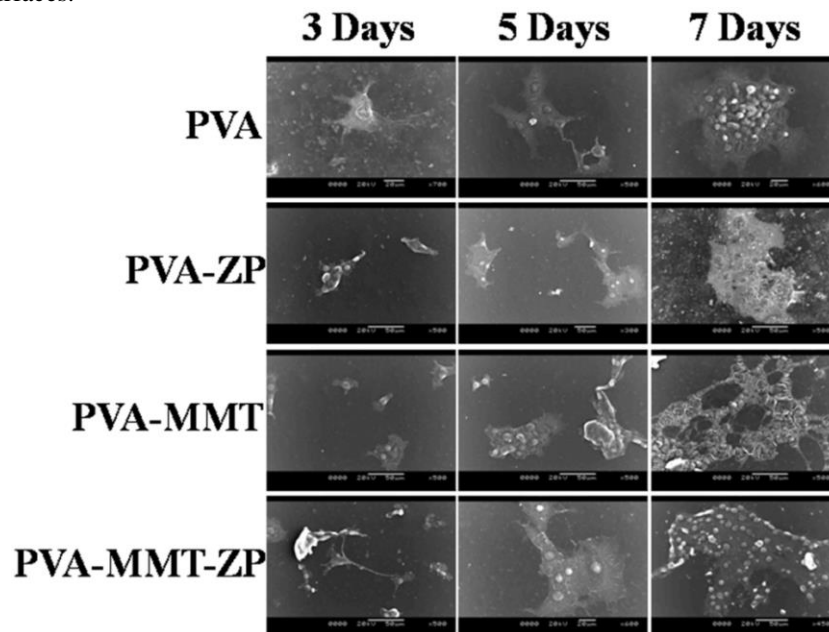


Fig. 12. SEM images of the nanocomposites attached with the 3T3 fibroblast cells.

The results of MTT assay and SEM analyses were further substantiated by the fluorescent images of the nanocomposites (attached with the cells) after 3, 5, and 7 days of culturing the cells. The fluorescent images showing the spreading and proliferation of the fibroblast cells on the nanocomposites' surface are presented in Fig. 13. It was observed that the blue fluorescence of the cells, stained with Hoechst 33342 dye, increases drastically with subsequent period of cell culture in all the nanocomposites, where the intensity was found to be highest in PVA-MMT-ZP followed by PVA-MMT, PVA-ZP, and neat PVA film at the end of 7th day.

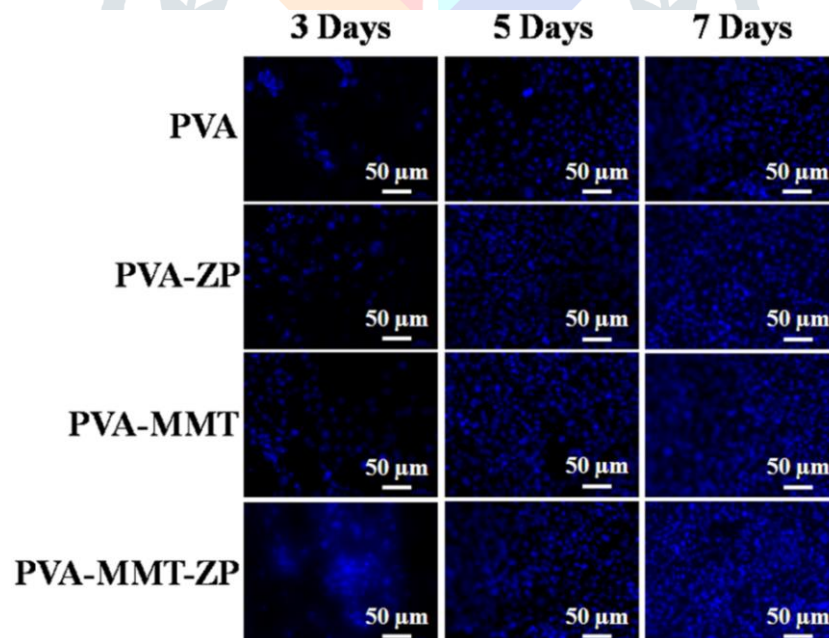


Fig. 13. Fluorescent images of the nanocomposites attached with the 3T3 fibroblast cells.

The results of MTT, SEM, and fluorescence microscopic analyses of the nanocomposites indicate that the nanocomposite of PVA with ZP and MMT (viz. PVA-MMT-ZP) provides a superior matrix material for the adhesion, spreading, and proliferation of cells in contrast to PVA-MMT, PVA-ZP, and neat PVA film. This superiority might have been aided by the presence of MMT (containing Mg and Ca) and ZP (containing phosphate) in the PVA-MMT-ZP nanocomposite in addition to the nanoroughness of its surface. Mg was reported to be closely linked with the mineralization of calcified tissues and indirectly influences the metabolism of minerals [32], while Ca and phosphorus are reported to be biomimetic and are helpful for cellular adhesion, proliferation, and migration [3]. As a result, PVA-MMT-ZP exhibits better bioactivity followed by PVA-MMT (containing MMT as filler) and PVA-ZP (containing ZP as filler). Thus, it can be inferred that the nanocomposite of PVA with MMT and ZP nanoparticles (viz. PVA-MMT-ZP) can serve as a potential matrix material in scaffold-guided tissue engineering application.

3.8. PROTEIN ADSORPTION STUDY

The BCA protein assay method of studying the adsorption of protein is based on the reduction of Cu^{2+} to Cu^{+} by the adsorbed proteins on the nanocomposites. The initial green coloration of the BCA reagent was changed to crimson color after the reduction of Cu^{2+} ions to Cu^{+} ions, which forms a complex with BCA (crimson coloration). The intensity of crimson coloration of the complex is proportional to the protein concentration which in turn, is a measure of the total amount of protein adsorbed on the nanocomposites. The results of protein adsorption study of the nanocomposites are shown in Fig. 14. It was observed that there is a considerable increase in protein adsorption level in all the nanocomposite films in contrast to the neat PVA film, where the adsorption is highest for PVA-MMT-ZP followed by PVA-MMT and PVA-ZP. It was also observed that the adsorption increases with increase in incubation period and maximum adsorption was found at 12 h for all the nanocomposites. Protein adsorption studies on scaffold is a qualitative assessment of cellular attachment on the scaffolds, since most mammalian cells are reported to be anchorage-dependent cells that requires biocompatible substrates for adhesion, migration and differentiation [33]. From the protein adsorption studies, it can be inferred that PVA-MMT-ZP nanocomposite film can serve as a promising matrix material for usage in scaffold-guided tissue engineering application.

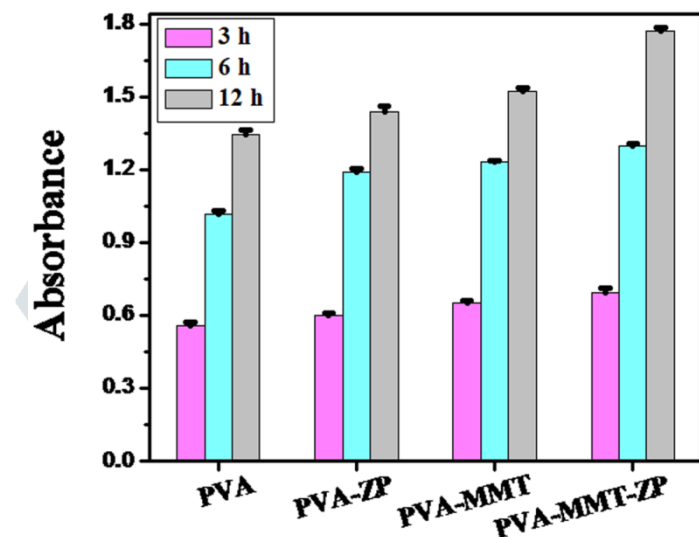


Fig. 14. Protein adsorption study of the neat PVA and nanocomposite films. Error bars represent the standard deviation from the mean (n=3).

4. CONCLUSIONS

Biocompatible polyvinyl alcohol/montmorillonite/zirconium phosphate nanocomposite film with improved nanomechanical properties (*viz.* hardness and elastic modulus) and higher bioactivity has been successfully prepared *via* solvent casting method for potential use as matrix in scaffold-guided tissue engineering application. The presence of MMT and ZP nanoparticles together, as fillers, improved both the mechanical properties as well as bioactivity of the nanocomposite film compared to the PVA/ZP, PVA/MMT nanocomposites and the neat PVA film. The PVA/MMT/ZP nanocomposite exhibited controlled biodegradation behavior and facilitated adhesion, proliferation and spreading of cells on its surface. The ease of fabrication, improved mechanical properties, higher bioactivity, controlled biodegradation as well as swelling behavior of the PVA/MMT/ZP nanocomposite film validated its potential as a suitable matrix material for scaffold-guided tissue engineering application.

REFERENCES

- [1] D. Sankar, K.P. Chennazhi, S.V. Nair, R. Jayakumar, Fabrication of chitin/poly(3-hydroxybutyrate-co-3-hydroxyvalerate) hydrogel scaffold, *Carbohydr. Polym.* 90 (2012) 725-729.
- [2] R.A. Hule, D.J. Pochan, Polymer nanocomposites for biomedical applications, *MRS Bull.* 32 (2007) 354-358.
- [3] D.X. Wang, Y. He, L. Bi, Z.H. Qu, J.W. Zou, Z. Pan, J.J. Fan, L. Chen, X. Dong, X.N. Liu, G.X. Pei, J.D. Ding, Enhancing the bioactivity of Poly(lactic-co-glycolic acid) scaffold with a nano-hydroxyapatite coating for the treatment of segmental bone defect in a rabbit model, *Int. J. Nanomed.* 8 (2013) 1855-1865.
- [4] H. Kalita, P. Pal, S. Dhara, A. Pathak, Fabrication and characterization of polyvinyl alcohol/metal (Ca, Mg, Ti) doped zirconium phosphate nanocomposite films for scaffold-guided tissue engineering application, *Mat. Sci. Eng. C* 71 (2017) 363-371.
- [5] C. Paluszkiwicz, E. Stodolak-Zych, W. Kwiatek, P. Jelen, Bioactivity of a chitosan based nanocomposite, *J. Biomim. Biomater. Tissue Eng.* 10 (2011) 95-106.
- [6] A. Olad, F.F. Azhar, The synergetic effect of bioactive ceramic and nanoclay on the properties of chitosan-gelatin/nanohydroxyapatite-montmorillonite scaffold for bone tissue engineering, *Ceram. Int.* 40 (2014) 10061-10072.
- [7] R.H.A. Haq, M.S. Wahab, M.U. Wahit, Impact test and bioactivity properties of polycaprolactone (PCL) by addition of nano-montmorillonite (MMT) and hydroxyapatite (HA), *Appl. Mech. Mater.* 446-447 (2014) 1129-1133.
- [8] Y. Yang, C. Liu, H. Wu, Preparation and properties of poly(vinyl alcohol)/exfoliated α -zirconium phosphate nanocomposite films, *Polym. Test.* 28 (2009) 371-377.
- [9] S.T. Bee, C.T. Ratnam, L.T. Sin, T.T. Tee, D. Hui, A.A.H. Kadhum, A.R. Rahmat, J. Lau, Effects of electron beam irradiation on mechanical properties and nanostructural-morphology of montmorillonite added polyvinyl alcohol composite, *Compos. Part B: Eng.* 63 (2014) 141-153.
- [10] A. Karimi, W.M.A.W. Daud, Harmless hydrogels based on PVA/Na⁺-MMT nanocomposites for biomedical applications: Fabrication and characterization, *Polym. Compos.* 38 (2017) 1135-1143.
- [11] W.B. Lawrimore, B. Paliwal, M.Q. Chandler, K.L. Johnson, M.F. Horstemeyer, Hierarchical multiscale modeling of polyvinyl alcohol/montmorillonite nanocomposites, *Polymer* 99 (2016) 386-398.
- [12] P.G. Allison, R.D. Moser, M.Q. Chandler, J.A. Caminero-Rodriguez, K. Torres-Cancel, O.G. Rivera, J.R. Goodwin, E.R. Gore, C.A. Weiss, Mechanical, thermal, and microstructural analysis of polyvinyl alcohol/montmorillonite nanocomposites, *J. Nanomater.* 2015 (2015) 291248.
- [13] Y. Ahmadian, A. Bakravi, H. Hashemi, H. Namazi, Synthesis of polyvinyl alcohol/CuO nanocomposite hydrogel and its application as drug delivery agent, *Polym. Bull.* 76 (2019) 1967-1983.
- [14] D. Ailincui, G. Gavril, L. Marin, Polyvinyl alcohol boric acid-A promising tool for the development of sustained release drug delivery systems, *Mat. Sci. Eng. C* 107 (2020) 110316.
- [15] M. Afshar, G. Dini, S. Vaezifar, M. Mehdikhani, B. Movahedi, Preparation and characterization of sodium alginate/polyvinyl alcohol hydrogel containing drug-loaded chitosan nanoparticles as a drug delivery system, *J. Drug Deliv. Sci. Technol.* 56A (2020) 101530.
- [16] M. Kobayashi, J. Toguchida, M. Oka, Development of the shields for tendon injury repair using polyvinyl alcohol-hydrogel (PVA-H), *J. Biomed. Mater. Res.* 58 (2001) 344-351.
- [17] C.J. Shuai, Z.Z. Mao, H.B. Lu, Y. Nie, H.L. Hu, S.P. Peng, Fabrication of porous polyvinyl alcohol scaffold for bone tissue engineering *via* selective laser sintering, *Biofabrication* 5 (2013) 015014.
- [18] M.M. Pillai, J. Gopinathan, R.S. Kumar, G.S. Kumar, S. Shanthakumari, K.S. Sahanand, A. Bhattacharyya, R. Selvakumar, Tissue engineering of human knee meniscus using functionalized and reinforced silk-polyvinyl alcohol composite three-dimensional scaffolds: Understanding the *in vitro* and *in vivo* behavior, *J. Biomed. Mater. Res. Part A* 106A (2018) 1722-1731.
- [19] S. Sheik, S. Sheik, R. Nairy, G.K. Nagaraja, A. Prabhu, P.D. Rekha, K. Prashantha, Study on the morphological and biocompatible properties of chitosan grafted silk fibre reinforced PVA films for tissue engineering applications, *Int. J. Biol. Macromol.* 116 (2018) 45-53.
- [20] L.C. Winterton, J.M. Lally, K.B. Sentell, L.L. Chapoy, The elution of poly (vinyl alcohol) from a contact lens: The realization of a time release moisturizing agent/artificial tear, *J. Biomed. Mater. Res. Part B Appl. Biomater.* 80B (2007) 424-432.
- [21] S. Saallah, M.N. Naim, I.W. Lenggono, M.N. Mokhtar, N.F.A. Bakar, M. Gen, Immobilisation of cyclodextrin glucanotransferase into polyvinyl alcohol (PVA) nanofibres via electrospinning, *Biotechnol. Rep.* 10 (2016) 44-48.
- [22] A.V. Penkova, S.F.A. Acquah, M.P. Sokolova, M.E. Dmitrenko, A.M. Toikka, Polyvinyl alcohol membranes modified by low-hydroxylated fullerene C₆₀(OH)₁₂, *J. Membr. Sci.* 491 (2015) 22-27.
- [23] R.V. Gadhav, P.S. Kashe, P.A. Mahanwar, P.T. Gadekar, To study the effect of boric acid modification on starch-polyvinyl alcohol blend wood adhesive, *J. Ind. Acad. Wood Sci.* 15 (2018) 190-198.
- [24] J.A. Killian, L.M. Geever, M. Cloonan, L. Grehan, C. Waldron, K. Quinn, J. Lyons, D.M. Devine, C.L. Higginbotham, Synthesis and photopolymerisation of maleic polyvinyl alcohol based hydrogels for bone tissue engineering, *J. Polym. Res.* 21 (2014) 538.
- [25] H. Kalita, B.N.P. Kumar, S. Konar, S. Tantubay, M.K. Mahto, M. Mandal, A. Pathak, Sonochemically synthesized biocompatible zirconium phosphate nanoparticles for pH sensitive drug delivery application, *Mat. Sci. Eng. C* 60 (2016) 84-91.
- [26] W.C. Oliver, G.M. Pharr, An improved technique for determining hardness and elastic modulus using load and displacement sensing indentation experiments, *J. Mater. Res.* 7 (1992) 1564-1583.
- [27] S. Gautam, C.F. Chou, A.K. Dinda, P.D. Potdar, N.C. Mishra, Surface modification of nanofibrous polycaprolactone/gelatin composite scaffold by collagen type I grafting for skin tissue engineering, *Mat. Sci. Eng. C* 34 (2014) 402-409.
- [28] S.K. Swain, T. Patnaik, V.K. Singh, U. Jha, R.K. Patel, R.K. Dey, Kinetics, equilibrium and thermodynamic aspects of removal of fluoride from drinking water using meso-structured zirconium phosphate, *Chem. Eng. J.* 171 (2011) 1218-1226.

- [29] A.M. Pandele, M. Ionita, L. Crica, S. Dinescu, M. Costache, H. Iovu, Synthesis, characterization, and in vitro studies of graphene oxide/chitosan-polyvinyl alcohol films, *Carbohydr. Polym.* 102 (2014) 813-820.
- [30] L. Jiang, X.P. Shen, J.L. Wu, K.C. Shen, Preparation and characterization of graphene/poly(vinyl alcohol) nanocomposites, *J. Appl. Polym. Sci.* 118 (2010) 275-279.
- [31] K.S. Katti, D.R. Katti, R. Dash, Synthesis and characterization of a novel chitosan/montmorillonite/hydroxyapatite nanocomposite for bone tissue engineering, *Biomed. Mater.* 3 (2008) 034122.
- [32] B. Bracci, P. Torricelli, S. Panzavolta, E. Boanini, R. Giardino, A. Bigi, Effect of Mg^{2+} , Sr^{2+} , and Mn^{2+} on the chemico-physical and in vitro biological properties of calcium phosphate biomimetic coatings, *J. Inorg. Biochem.* 103 (2009) 1666-1674.
- [33] G. Wei, P.X. Ma, Structure and properties of nano-hydroxyapatite/polymer composite scaffolds for bone tissue engineering, *Biomaterials* 25 (2004) 4749-4757.

